

## Article

# Types and Genesis of Siderite in the Coal-Bearing Beds of the Late Permian Xuanwei Formation in Eastern Yunnan, China

Hailei Tang <sup>1</sup>, Qing Zhao <sup>2</sup>, Bo Liu <sup>2,3,\*</sup>, Shucheng Tan <sup>3</sup> and Kaibo Shi <sup>2</sup><sup>1</sup> Institute of International Rivers and Eco-Security, Yunnan University, Kunming 650500, China<sup>2</sup> School of Earth and Space Sciences, Peking University, Beijing 100871, China<sup>3</sup> School of Earth Sciences, Yunnan University, Kunming 650500, China

\* Correspondence: bobliu@pku.edu.cn

**Abstract:** The Late Permian strata of the Xuanwei Formation in the eastern Yunnan region exhibit extensive diverse morphological features within siderite deposits. These variations in siderite deposits suggest potential differences in their formation processes. In this study, fieldwork and comprehensive indoor studies revealed four distinct forms of siderite deposits: stratiform-laminated, lens-like nodule, sandstone cementation, and fracture filling. The stratiform-laminated siderite, varying in color from bluish-grey to dark grey, is composed of uniformly sized microcrystalline to fine-grained siderite along with detrital matter, displaying precise layering and banding structures that suggest direct deposition from cyclic iron-rich seawater under reducing conditions. Lens-like-nodule siderite, which appears grey-yellow, is composed of mud microcrystalline siderite, medium to coarse-grained pseudo-ooids, and glauconite. It shows conformable distribution characteristics resulting from the diagenetic differentiation of iron-rich sediments under reducing conditions during the diagenetic and early diagenetic periods. Siderite as sandstone cementation exhibits a yellow-brown color and consists of dispersed colloidal siderite and cemented siderite clumps that fill intergranular pores of detrital particles. It precipitated under reducing conditions within those intergranular pores. Siderite filling fractures typically appear as vein-like or network-like structures intersecting bedding at large angles. They exhibit grain structures with significant variations in size. These siderite deposits exhibit exceptional purity and result from siderite dissolution during sedimentary periods, followed by reprecipitation within regional extensional fractures during the diagenetic phase. The primary occurrence of siderite deposits in the study area is within coal-bearing strata, as revealed by the integration of sedimentary profiles and sedimentary facies analysis. The coal-bearing strata, influenced by the Emeishan large igneous province, underwent iron enrichment during and after volcanic eruptions while developing a reducing environment, which was facilitated by abundant vegetation. Consequently, geological processes led to siderite layers, lens-like siderite nodules, and siderite cementation. The Yanshan orogeny induced extensive high-angle fracture development in epigenetic coal-bearing strata, facilitating fluid circulation and the redistribution of soluble siderite. This geological activity resulted in the formation of vein-like structures composed of siderite.

**Keywords:** eastern Yunnan; Xuanwei Formation; siderite; types and genesis

**Citation:** Tang, H.; Zhao, Q.; Liu, B.; Tan, S.; Shi, K. Types and Genesis of Siderite in the Coal-Bearing Beds of the Late Permian Xuanwei Formation in Eastern Yunnan, China. *Minerals* **2023**, *13*, 1233. <https://doi.org/10.3390/min13091233>

Academic Editors: Magdalena Misz-Kennan, Monika J. Fabiańska, Justyna Ciesielczuk and Marek Szczerba

Received: 9 August 2023

Revised: 8 September 2023

Accepted: 12 September 2023

Published: 21 September 2023



**Copyright:** © 2023 by the authors. Licensee MDPI, Basel, Switzerland. This article is an open access article distributed under the terms and conditions of the Creative Commons Attribution (CC BY) license (<https://creativecommons.org/licenses/by/4.0/>).

## 1. Introduction

Siderite possesses considerable economic value and serves as an essential environmental indicator of unique significance [1]. In the past, researchers primarily relied on geochemical methods to explore the genesis mechanism of siderite deposits. However, recent studies suggest that conducting detailed petrological analysis can provide invaluable insights into the formation process of siderite [2–4]. Siderite deposits exhibit a wealth of occurrences across diverse stratigraphic horizons and have a prolonged mineralization history. The stratigraphic position influences their geological characteristic and has a fundamental role [5]. Based on their sedimentary environments and genetic types, siderite deposits

can be categorized as follows: (1) direct precipitation in marine carbonate sedimentary environments [6,7]; (2) formation through the interaction of marine sedimentation and volcanic activities [8]; (3) coexistence with sandstone and mud shale in marine-continental transitional environments [9]; (4) cementation in sandstone and conglomerate within lacustrine Molasse formations [10]. The influence of sedimentary and diagenetic environments significantly contributes to the occurrence of siderite, leading to the formation of diverse mineral associations in distinct sedimentary settings [11,12].

The Late Permian coal-bearing area in eastern Yunnan is located in the southwestern part of the Yangtze Plate. It is characterized by distinct sedimentary layer sequences, a relatively stable terrestrial supply, and well-developed fold–fault structures [13]. Siderite is present in the outcrops in our study area. To date, researchers have concentrated on investigating siderite within these coal-bearing strata, undertaking research related to resource exploration and environmental evolution [14,15]. Numerous scholars have conducted comprehensive studies on siderite in coal-bearing strata, aiming to explore the accumulation and evolution of coalbed methane in southern China and the occurrence status and controlling mechanisms of shale gas in marine-continental transitional environments [16–20]. The present study centers on siderite deposits in eastern Yunnan in Late Permian Xuanwei Formation coal-bearing strata. Employing field outcrop observations, microscopic examinations, and geochemical analysis, this research aims to identify the genetic types of siderite deposits within coal-bearing strata and analyze their sedimentary and diagenetic environmental characteristics.

## 2. Regional Geological Setting

The study site is situated in the eastern Yunnan-Guizhou coal accumulation zone, which lies in the southwestern region of the Yangtze Plate (Figure 1A) [21]. The Late Mesozoic Yanshan Movement resulted in the development of a complex fault system within the region. The primary faults comprise the Xiaojiang Fault, trending north–south, the Shuicheng Fault, trending northwest, the Mile-Shizong Fault, trending northeast, and the Xiaganhe Fault (Figure 1A). These faults act as boundaries between the South China Permian coal basins and the Kangdian ancient land, and also served as conduits for Late Permian Emeishan basaltic lava flows (Figure 1D). During the Paleozoic to Triassic periods, carbonate rock deposition prevailed, with the Permian and Triassic periods exhibiting the most extensive and widespread development (Figure 1B).

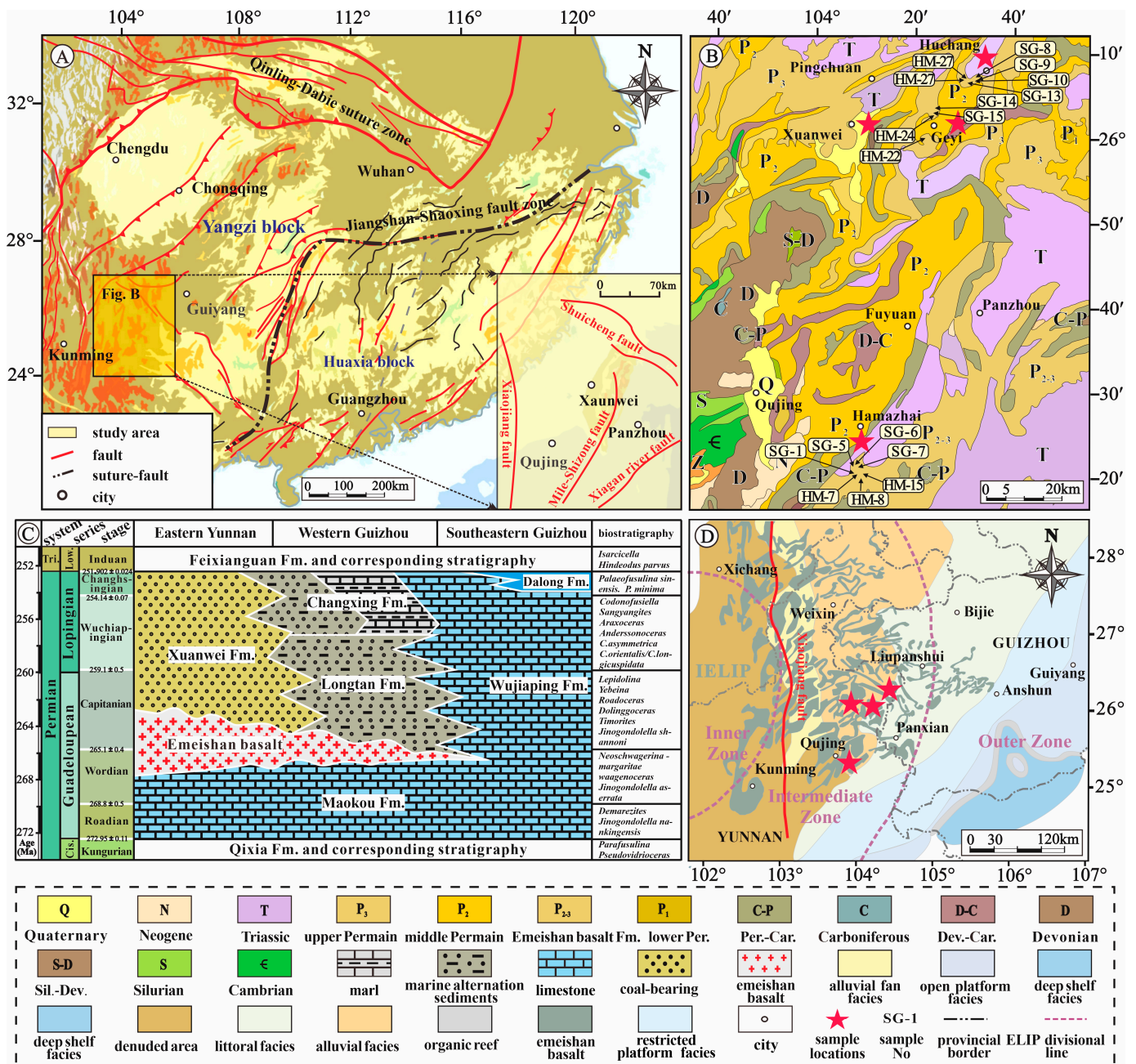


**Figure 1.** Regional tectonic and sedimentary zoning of the study area. (A) Simplified structural chart of tectonic zoning in southern China and the study area’s structural map (modified from [21]); (B) geological map of eastern Yunnan (redrawn from the 1:200,000 geological map of Yunnan Province, 1965); (C) comprehensive lithostratigraphic and chronostratigraphic chart of Permian rocks in southwestern China (modified from [22,23]); (D) Late Permian Xuanwei Formation sedimentary paleogeography and distribution of the Emeishan large igneous province in western Yunnan and eastern Guizhou (modified from [24,25]).

Figure 1C illustrates the Late Permian stratigraphic division in the study area. The Upper Permian comprises two stages: Wuchiapingian and Changhsingian. The Wuchiapingian stage includes the Emeishan Basalt Formation and Longtan Formation, with the Longtan Formation and the middle-lower Xuanwei Formation or the Wuchiapingian Formation being contemporaneous heterogeneous sedimentary strata [23]. The lower section of the Emeishan Basalt Formation is mainly composed of a series of bare continental volcanic rocks that unconformably overlie the limestone of the Maokou Formation. The Longtan

Formation, predominantly composed of sandstone and mudstone, contains significant coal seams, carbonaceous mudstone, and localized thin limestone layers, making it the most crucial coal-bearing stratum in the southwestern region. The Changhsingian Stage includes the Changhsingian Formation and the upper section of the Xuanwei Formation. The Xuanwei Formation, proposed by Xie et al. [26], represents Late Permian continental coal-bearing deposits in eastern Yunnan. It unconformably contacts the underlying basalt formation. The measured Late Permian Xuanwei Formation coal-bearing strata, including siderite layers, are predominantly distributed in the study area's transitional zone between marine and terrestrial environments. Geographically, these strata transition from alluvial plains in the west to nearshore facies in the shallow water area towards the east (Figure 1D) [24,25].

### 3. Samples and Methods

Fifty-nine samples from the Late Permian Xuanwei Formation were gathered in diverse locations, encompassing fresh stratiform-laminated siderite, lens-like nodule, sandstone cementation, and fracture filling samples. We executed a systematic, layer-by-layer sampling approach within the stratiform-laminated siderite outcrop region—for other types of siderite, fresh block samples were acquired, including Hamazhai, Geyi, and Huchang Town samples in eastern Yunnan. Petrological work was primarily conducted at the School of Earth Sciences, Yunnan University, utilizing microscopic observations to summarize the characteristics of siderite. Major elemental analysis of samples was carried out at the Chongqing Key Laboratory of Paleontology and Paleoenvironment Co-evolution (Sichuan-Chongqing Joint Construction). Before significant elemental analysis, fresh samples weighing 50 g were dried in an oven for 24 h and ground to 200 mesh. The ground powder was blended with a boric acid binder and pressed into pellets with a diameter of 40 mm and a thickness of 10 mm using a pellet press. Subsequently, X-ray fluorescence spectrometry (XRF) was used for significant element analysis, achieving an experimental relative error of less than 2%. XRF elemental analysis was used to help identify the sedimentary environment of siderite.

## 4. The Attitude and Characteristics of Siderite

### 4.1. Stratiform-Laminated Siderite

Stratiform-laminated siderite is extensively distributed in the Hamazhai section of Qujing City. This section fundamentally represents the lithological and biotic assemblage characteristics of the Xuanwei Formation in the study area. The late Permian Xuanwei Formation is extensively exposed, with a thickness exceeding 50 m [27]. The lithology mainly comprises purple-red sandstone, gray-yellow fine sandstone, siltstone, tuffaceous sandstone, mudstone, siderite, and coal seams, which are parallel and unconformably overlain by basaltic rocks (Figure 2A). The lowermost layer of the section consists of the late Permian Emeishan basalt formation, exhibiting a gray-green coloration. The formation has a thickness exceeding 5 m; it is exposed in places, and otherwise it is extensively covered. The lower part of the Xuanwei Formation is mainly composed of a dense purple-red ferruginous sandstone containing interbedded plant-fragment fossils. The middle section consists of gray to gray-yellow fine sandstones interbedded with siltstone, tuffaceous sandstone, mudstone, siderite layers, and six coal seams with a thickness ranging from 0.4 to 1 m. The upper-middle part displays yellow, medium to coarse-grained rhombohedral iron-rich sandstone, rhythmically interbedded with yellow-green mudstone, shale, and carbonaceous shale (Figure 2B). The thickness of individual siderite deposits ranges from 5 to 8 cm, displaying bluish-gray to dark gray coloration, characterized by a hard texture (Figure 2C) and exhibiting lateral stability. The uppermost layer of the Xuanwei Formation contains a set of bluish-gray conglomerates with thicknesses of 0.5 to 1 m.

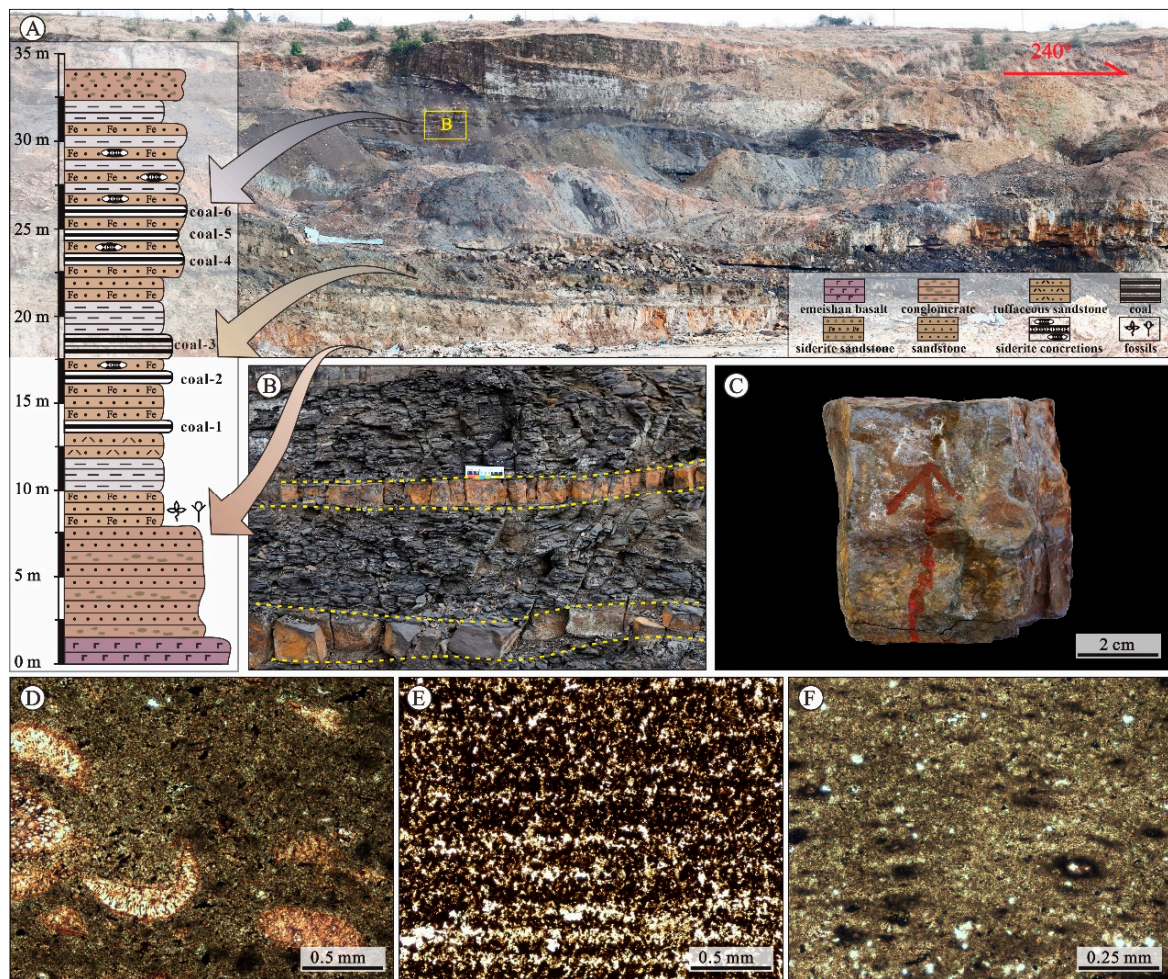


**Figure 2.** Microscopic characteristics of stratiform-banded siderite in the Hamazhai section of Qujing City. (A) The outcrop of stratiform-banded siderite in the coal-bearing rock series is observed at a macroscopic level, accompanied by a lithological column illustration on the left side; (B) the siderite, distributed in a banded pattern within the coal-bearing strata, exhibits a yellowish-brown coloration; (C) a magnified photograph of a specific area from (B) is provided; (D) the microcrystalline to fine-grained siderite contains bioclasts, such as foraminifera and algae, HM-8,  $\times 5$ ; (E) the microcrystalline to fine-grained siderite exhibits lamination and banded structures, HM-13,  $\times 5$ ; (F) an aggregation of micro-powdery siderite is observed, HM-15,  $\times 5$ .

The stratiform-banded siderite consists of uniform-sized microcrystalline to fine-grained siderite and mudstone. It frequently contains bioclasts such as foraminifera and algae, as shown in Figure 2D. The rock comprises various components, including clay minerals, clastic materials, siliceous materials, carbonaceous materials, and siderite, distributed parallel to the layers, manifesting lamination and banded structures. Distinct zonations are evident, and fine disseminated pyrite is observable between layers, as illustrated in Figure 2E. Under the microscope, the microcrystalline to fine-grained siderite exhibits clear particle boundaries and appears light yellow, forming an aggregation of microcrystalline siderite with varying-sized subhedral to euhedral forms, as depicted in Figure 2F. Chemically, it is characterized by a low  $\text{Fe}_2\text{O}_3^{\text{T}}$  (total iron content represented in  $\text{Fe}_2\text{O}_3$ ), averaging 9.87 wt%, and a high  $\text{K}_2\text{O}$  content, with an average of 0.25 wt% (Table 1).

**Table 1.** Major-element oxides in rhombohedral iron ore from the Late Permian Xuanwei Formation of the eastern region in Yunnan (wt%).

Types	Sample No.	SiO <sub>2</sub>	TiO <sub>2</sub>	Al <sub>2</sub> O <sub>3</sub>	Fe <sub>2</sub> O <sub>3</sub>	MnO	MgO	CaO	K <sub>2</sub> O	P <sub>2</sub> O <sub>5</sub>	LOI
Fracture filling	SG-15	17.6	0.93	5.86	63.44	0.61	0.7	2.05	0.12	1.58	7.11
	SG-14	12.65	2.42	11.8	63.1	0.11	0.69	2.32	0.4	1.81	4.70
	SG-7	18.38	3.51	8.68	58.91	0.03	—	0.02	0.09	1.14	9.24
	average	16.21	2.29	8.78	61.82	0.25	0.70	1.46	0.20	1.51	6.79
Lens-like and nodule siderite	HM-22	11.98	0.92	9.28	59.93	1.7	1.81	1.95	0.12	0.31	12.00
	HM-24	14.22	1.28	8.46	54.23	0.96	2.64	4.92	0.24	1.31	11.74
	SG-6	27.59	0.2	3.51	53.35	0.28	0.03	0.06	0.03	0.3	14.65
	SG-13	27.85	1.53	16.3	39.93	0.07	0.26	0.13	0.02	2.03	11.88
	HM-30	34.16	2.28	16.42	36.17	0.95	2.41	2.31	0.83	0.51	3.96
	SG-5	24.79	2.07	19.65	34.62	0.09	0.7	0.59	0.07	3.69	13.73
	SG-9	25.37	0.09	11.97	32.49	—	—	0.03	0.05	0.05	19.95
average	23.71	1.20	12.23	44.39	0.68	1.31	1.43	0.19	1.17	13.70	
Stratiform-laminated siderite	SG-1	25.02	0.9	15.65	14.9	0.06	0.5	0.39	0.03	1.4	21.15
	HM-15	22.76	2.73	28.88	7.81	0.06	0.13	0.3	0.46	0.41	26.46
	HM-8	26.4	1.82	39.22	6.89	—	0.13	1.72	—	2.08	21.74
	average	24.73	1.82	27.92	9.87	0.06	0.25	0.80	0.25	1.30	13.02
Sandstone cementation	HM-27	36.36	6.99	29.27	6.42	0.07	0.2	0.05	0.28	0.13	15.23
	HM-7	28.17	12.21	43.06	4.32	—	0.08	0.05	0.09	0.46	11.56
	SG-10	46.96	2	35.64	2.83	0.05	0.04	0.03	0.11	0.07	12.27
	SG-8	49.84	1.77	36.63	2.05	0.05	0.04	0.03	0.11	0.09	9.39
	average	40.33	5.74	36.15	3.91	0.06	0.09	0.04	0.15	0.19	13.35

#### 4.2. Lens-like and Nodule Siderite

The Geyi section of Qujing City contains lens-like and nodule siderite. At the section's bottom are purple basaltic tuffaceous siltstones developed from the Emeishan Basalt Formation (Figure 3A), which exhibit well-developed pores and a sedimentary thickness exceeding 2 m. The lower to middle part of the Xuanwei Formation consists of sequentially developed light gray mudstone, aluminous mudstone, and marl. At a depth of 2.5 m from the section's bottom, a coal seam with a thickness of 0.5 m is found, characterized by high and unstable ash content. In the middle part of the section, lens-like and nodule siderite can be observed (Figure 3A), appearing as protruding lenses and nodules after weathering (Figure 3B,D). The lens-like and nodule siderite is laterally distributed parallel to the layers, exhibiting relative stability and continuity. At the section's top, a 0.5 m thick interbed of clayey limestone is present (Figure 3A).

Lens-like siderite displays a bluish-gray fresh surface and is distributed along layers, as shown in Figure 3B. Microscopic examination reveals the coexistence of some siderite with glauconite and apatite (Figure 3C). Following weathering, the siderite nodules display a yellowish-brown weathering surface, with concentric circular structures formed by iron and sandy–muddy materials. A brown oxidized crust encloses the same sandstone as the surrounding rock (Figure 3D). Oxidation causes the development of a yellowish-brown membrane on siderite crystals. Exposure and leaching lead to well-developed dissolution pores. Clay impurities contribute to a darker coloration (Figure 3E). Figure 3F displays relatively well-preserved and fresh, large siderite nodules with a gray-green surface and measuring 15–20 cm in diameter. Under plane-polarized light, they appear yellowish-brown and consist of medium to coarse, subhedral spherical grains, with grain sizes ranging from 0.1 to 0.5 mm, some of which exhibit petal-like structures—these nodules also exhibit good crystallinity. In terms of chemical composition, they are characterized by lower Fe<sub>2</sub>O<sub>3</sub><sup>T</sup> content (averaging 44.39 wt%), higher P<sub>2</sub>O<sub>5</sub> (average 1.17 wt%), higher MnO (average 0.68 wt%), and lower TiO<sub>2</sub> (average 1.20 wt%) than fracture-filled siderite, as shown in Table 1.

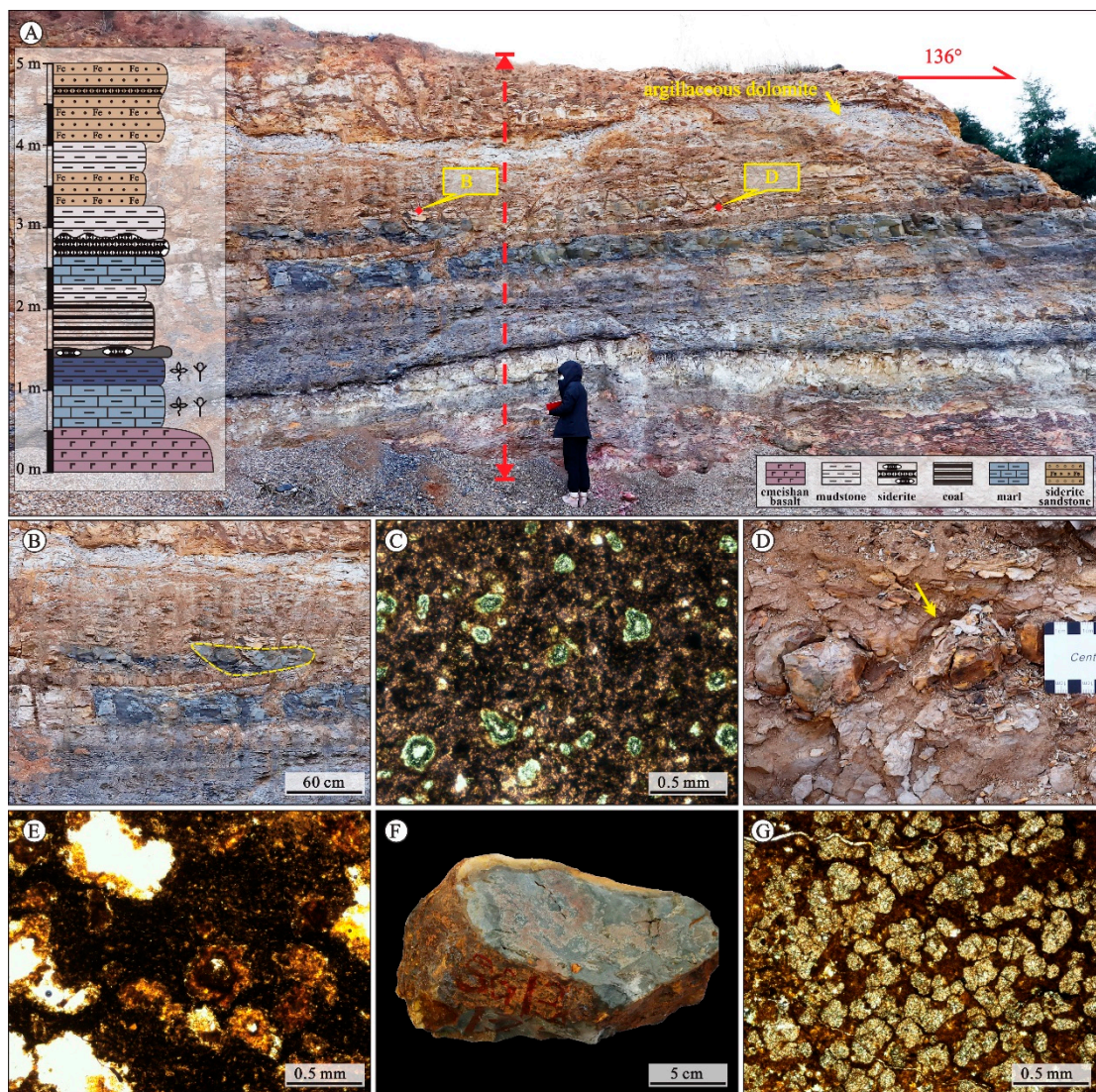


**Figure 3.** Macroscopic and microscopic features of lens-like and nodule siderite at the Geyi section are examined. (A) The coal-bearing rock series of siderite is macroscopically exposed, with the lithological column illustrated in the left-side sketch; (B) macroscopic photograph of lens-like siderite, displaying a fresh bluish-gray surface; (C) microscopic phenomena of lens-like siderite, coexisting with glauconite and apatite, HM-22,  $\times 5$ ; (D) macroscopic photograph of nodular siderite is presented; (E) microscopic phenomena of nodular siderite, consisting of microcrystalline siderite, SG-5,  $\times 5$ ; (F) photograph of large-grained siderite nodules is presented, SG-13; (G) microscopic phenomena of nodular siderite, exhibiting medium to coarse-grained siderite,  $\times 5$ .

#### 4.3. Sandstone Cementation

In the northeastern part of the study area, specifically at the Huchang Town section, the lithology of the Xuanwei Formation's coal-bearing rock series predominantly comprises yellowish-brown ferruginous sandstone, marl, gray claystone, and interbedded thick layers of rhombohedral iron-rich sandstone, which exhibit a thickness ranging from 7 to 11 m and include one coal seam. Towards the bottom of the section, moderately thick layers of gray mudstone, calcareous fine sandstone, fine sandstone, and claystone are encountered. At the same time, the upper part is characterized by thin layers of gray-yellow fine sandstone, rhombohedral iron-rich fine sandstone, and mudstone (Figure 4A,B). The siderite is found as cementing material within sandstone layers, and the thickness of the sandstone varies between 0.5 and 1 m. Initially, the fresh surface displays a light grayish-green hue, but with weathering, it changes to a yellow-green color (Figure 4C).

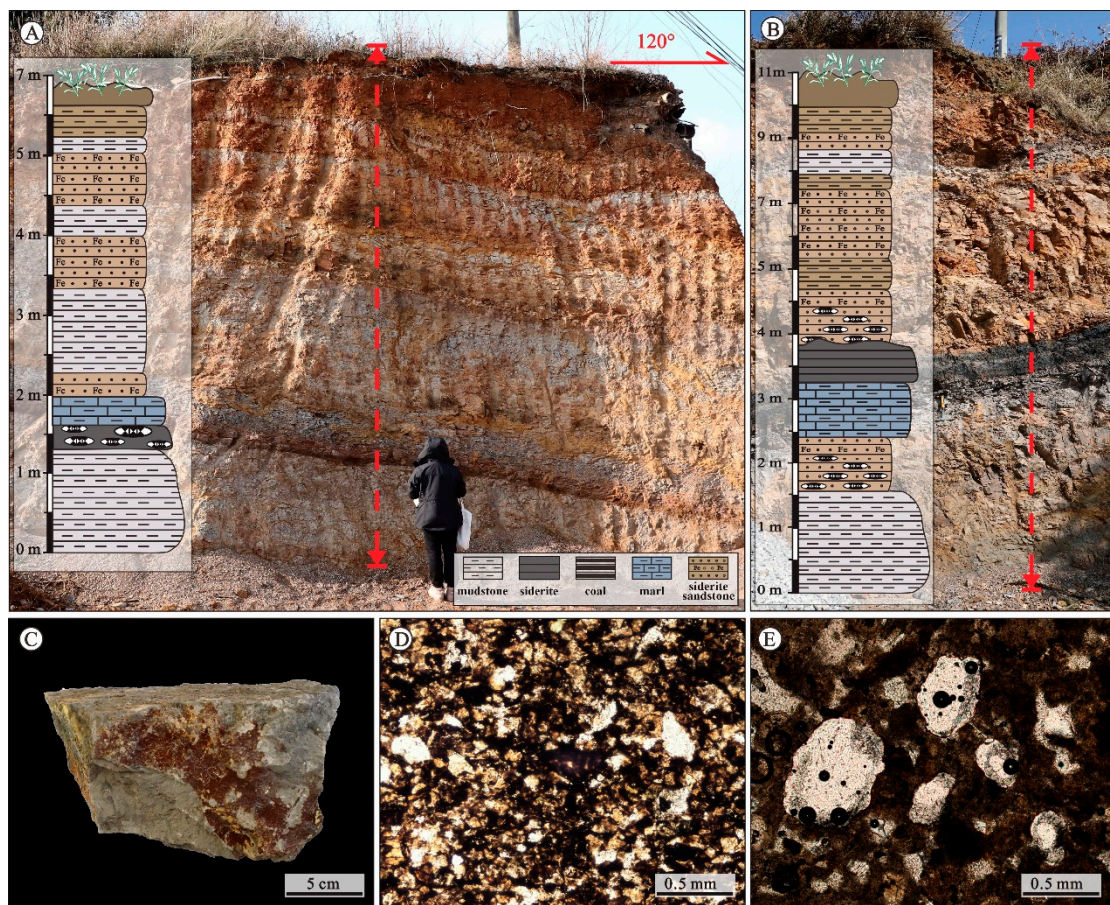


**Figure 4.** Macroscopic and microscopic characteristics of siderite as a cementing material in sandstone at the Huchang Town section. (A,B) Coal-bearing strata expose a layer of siderite—the accompanying left-hand sketch illustrates the lithological column; (C) macroscopic photograph of sandstone containing rhombohedral iron, SG-10; (D) microscopic characteristics of agglomerated colloform siderite, SG-8,  $\times 5$ ; (E) microscopic features of dispersed agglomerated siderite, SG-10,  $\times 5$ .

The morphology of siderite cement in iron ore predominantly consists of massive siderite aggregates and dispersed siderite aggregates. The material composition of the massive siderite aggregates is relatively simple, primarily comprising a mud-like microcrystalline structure of siderite. Additionally, aggregates contain significant amounts of sand, silt, and minor carbonaceous materials (Figure 4D). Dispersed siderite aggregates exhibit a brownish-yellow color under both plane-polarized and cross-polarized light microscopy. They are dispersed within the rock, frequently filling the pores between debris particles as cement (Figure 4E). This type of siderite is characterized by a low  $\text{Fe}_2\text{O}_3^{\text{T}}$  content, averaging 3.91 wt%, and relatively high contents of  $\text{Al}_2\text{O}_3$  (average 36.15 wt%),  $\text{SiO}_2$  (average 40.33 wt%), and  $\text{TiO}_2$  (average 5.74 wt%) (Table 1).

#### 4.4. Fracture Filling

Abundant fracture-filled siderite was observed in multiple profiles within the study area, frequently found along joint surfaces (usually perpendicular to the bedding plane) and fractures, with its orientation influenced by the intersection of distinct joint sets. Fracture-filled siderite typically measures between 1 and 2 cm in width, displaying a reddish-brown color after weathering, and a light gray hue when fresh (Figure 5A). Fracture fillings have a high density, forming a grid-like pattern resulting from the intersection of joints and fractures, which leads to the formation of mesh-like siderite aggregates (Figure 5B). Siderite developed within fractures frequently exhibits a grape-like form under the microscope, with grain sizes ranging from 20 to 40  $\mu\text{m}$  (Figure 5C). Filamentous sand and grape-like

siderite aggregates are observed together (Figure 5D), while laminated fine to medium-sized siderite coexists with grape-like siderite (Figure 5E). This type of siderite exhibits the highest  $\text{Fe}_2\text{O}_3^{\text{T}}$  content, averaging 61.82 wt%, along with elevated levels of  $\text{P}_2\text{O}_5$  (average 1.15 wt%) and CaO (average 1.46 wt%) (Table 1).

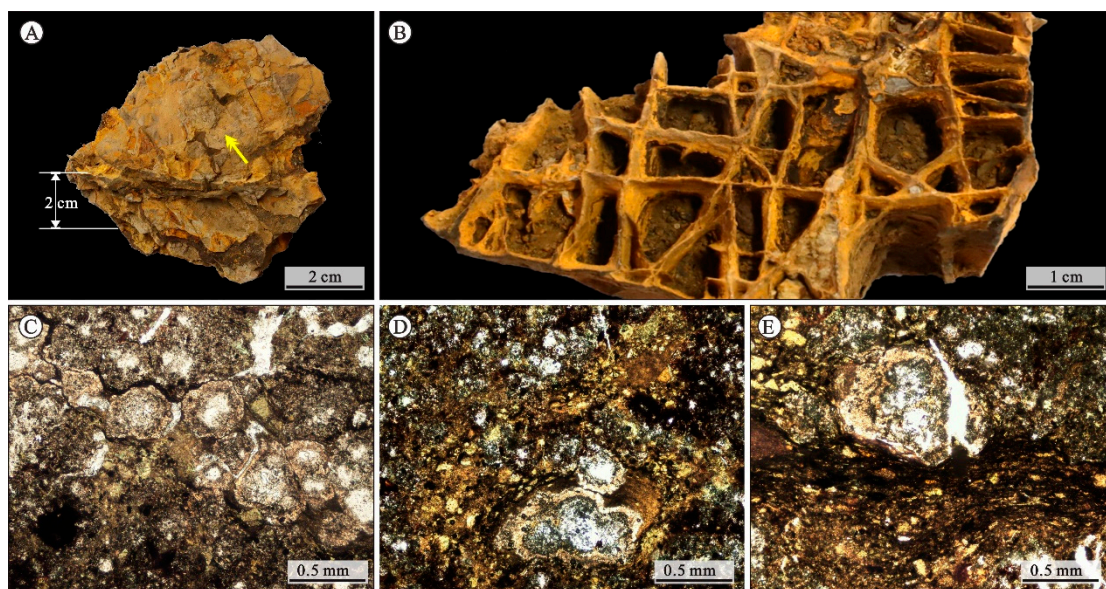


**Figure 5.** The macroscopic and microscopic characteristics of siderite developed within tectonic fractures. (A) Siderite developed within fractures and joint surfaces; (B) photograph of mesh-like structured siderite; (C) Microscopic characteristics of grape-like siderite, SG-7,  $\times 5$ ; (D) microscopic characteristics of grape-like siderite coexisting with infiltrated sand, SG-14,  $\times 5$ ; (E) microscopic characteristics of grape-like siderite coexisting with laminated fine to medium-sized siderite, SG-15,  $\times 5$ .

In conclusion, the late Permian Xuanwei Formation in the study area exhibits a wealth of siderite deposits within coal-bearing strata. The prevailing colors range from gray to dark gray and yellow-brown. Siderite is found in various forms, such as stratiform-laminated and lens-nodular structures. It is commonly found as cementation within sandstone and fracture filling.

## 5. Genesis of Siderite in Coal-Bearing Beds

Siderite deposits are most abundant and have the largest reserves during significant coal-forming periods, such as the Carboniferous, Permian, Jurassic, Cretaceous, and other geological eras [28–30]. A systematic lithofacies analysis identified four types of siderite deposits within the Xuanwei Formation coal-bearing strata in the study area, distinguished by their occurrence characteristics: layered-striated, lens-nodular, sandstone cementation, and fissure fillings. The varied occurrences of siderite may indicate differences in their genesis, as this common authigenic mineral can form in various sedimentary and diagenetic environments [5,31].

### 5.1. Sedimentary Genesis

Siderite typically forms during the diagenetic stage of a typical sedimentary sequence, requiring a constant supply of  $\text{Fe}^{2+}$  and a persistent reducing environment for a specific duration [32]. The layered-striated siderite developed in the study area is frequently associated with organic matter, including coal beds, carbonaceous shales, and mudstones. The reducing action of organic matter converts  $\text{Fe}^{3+}$  in diagenetic fluids to  $\text{Fe}^{2+}$ , thereby providing a continuous source of  $\text{Fe}^{2+}$ . This  $\text{Fe}^{2+}$  reacts with  $\text{CO}_2$  generated from the decomposition of organic matter, forming  $\text{FeCO}_3$  [20]. The relationship diagram of MgO and

CaO (Figure 6A) shows a positive correlation between their content (correlation coefficient  $R = 0.7551$ ). The mass fraction ratio ranges from 0.07 to 13.54 (average of 1.81), indicating that the Xuanwei Formation formed in a warm and humid climate in a brackish-water marine–terrestrial transitional environment. The distribution map of the transition elements V/Cr and V (V + Ni) (Figure 6B) indicates siderite formation in a hypoxic to anoxic environment. These conditions resulted in the construction of uniform, fine-crystalline siderite with shades of bluish-gray to dark gray. Laminae and layered structures indicate significant sedimentary control, reflecting the cyclic direct deposition of iron-rich seawater under reducing conditions.

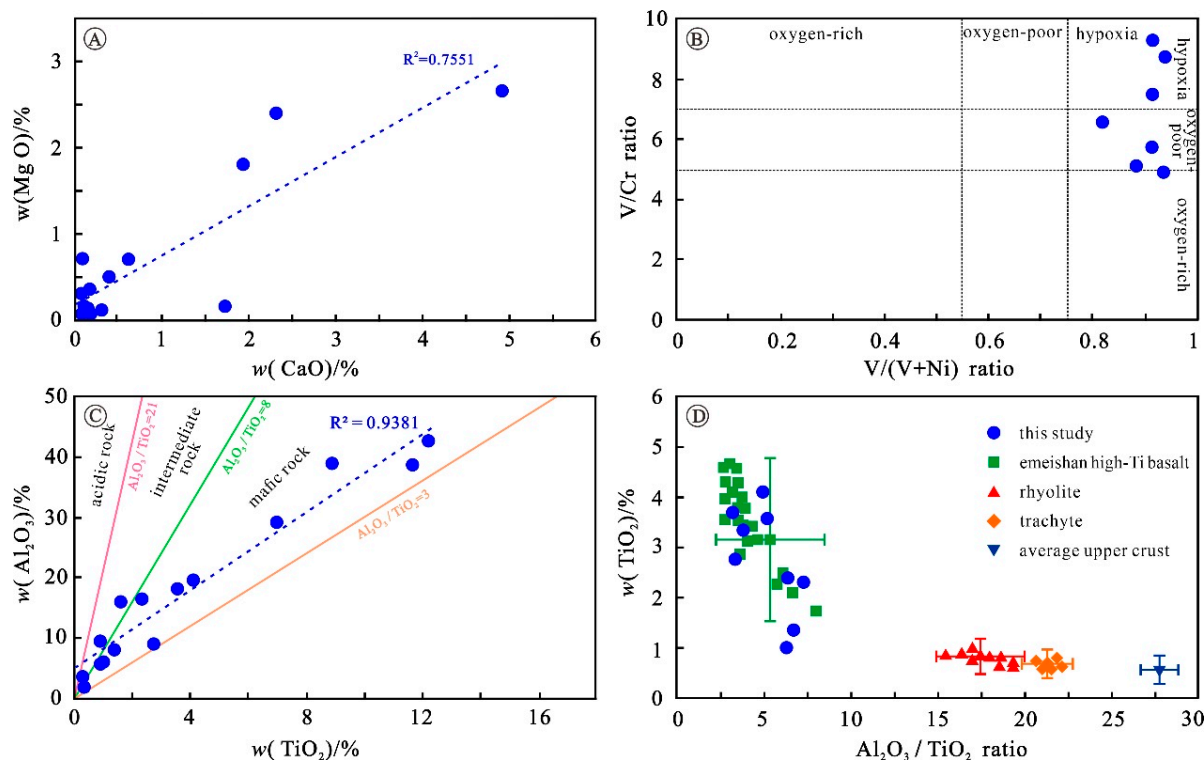


**Figure 6.** Comprehensive geochemical characterization map of siderite in the Late Permian Xuanwei Formation coal-bearing strata in Eastern Yunnan. (A) Siderite’s major-element binary diagram of MgO and CaO; (B) distribution map of transition elements’ V/Cr and V (V + Ni) ratios in siderite; (C) binary diagram of major elements Al<sub>2</sub>O<sub>3</sub> and TiO<sub>2</sub> in siderite; (D) Al<sub>2</sub>O<sub>3</sub>/TiO<sub>2</sub>-TiO<sub>2</sub> diagram of major elements in siderite and comparisons with Emeishan igneous rock composition.

The diagenetic environment extends and continues the sedimentary environment. During the shallow burial stage, poorly sorted mixed systems develop into lenses and nodules (Figure 3). Siderite and chlorite in a ring-shaped ooid are not due to alternating oxidation and reduction conditions in turbulent shallow-water environments. Instead, they are formed during the same period through the diagenetic alteration of iron hydroxides and iron and organic-matter-rich clay layers. Under the influence of diagenetic differentiation, these features experience in situ alteration and differentiation processes without significant transport or re-deposition over distance. Iron-rich diagenetic fluids directly influence them under reducing conditions during early and syn-diagenetic periods.

### 5.2. The Early Diagenetic Cementation Genesis

Siderite present in sandstone and siltstone, regardless of its cementation mode, indicates specific reducing environments and is influenced by the oxidation–reduction potential balance in the environment [10]. Simultaneously, the reducing agent responsible for iron reduction is associated with organic matter from coal-bearing strata enriched in

marine–terrestrial transition zones. Under these reducing conditions, siderite, acting as a cementing material in sandstone, exhibits a yellow-brown color and consists of dispersed siderite aggregates and massive siderite clasts. It fills intergranular pores between debris particles in the form of cement, formed by the precipitation of siderite from seawater under reducing conditions within the intergranular pores of sand grains.

The  $\text{TiO}_2$  content in the overall siderite samples from the study area ranges from 0.04 to 0.3, with the highest  $\text{TiO}_2$  content observed in siderite cementation.  $\text{TiO}_2/\text{Al}_2\text{O}_3$ - $\text{TiO}_2$  ratio plots reveal that the distribution is mainly concentrated in mafic rock regions (Figure 6C). The samples exhibit significant similarity with the high-Ti basalt of ELIP [33–35] (Figure 6D), while displaying apparent differences from the compositions of rhyolite, coarse-grained rocks [36] and the average continental crust [36,37]. Based on these findings, we infer that the overlying Emeishan basalt of the Xuanwei Formation serves as the material source for the formation of siderite in the coal-bearing strata, which is influenced by weathering and erosion. Consequently, this leads to higher  $\text{TiO}_2$  content in the roof, floor, and regularly deposited siderite (Table 1), aligning with earlier suggestions regarding the area's provenance having both alkaline and ferromagnesian origins [38,39].

### 5.3. The Origin of Epigenetic Dissolution and Filling

During the Yanshan orogeny, tectonic uplift led to structural fractures which were influenced by regional main faults [40], creating a favorable physical space for developing siderite filling within these fractures. The diagenetic siderite in the surrounding rocks undergoes short-distance migration and precipitates along joints and fractures, cutting across bedding planes and giving rise to vein-like and mesh-like siderite structures that intersect the strata at significant angles (Figure 5A,B). Simultaneously, fractures facilitate the weathering, oxidation, and precipitation of  $\text{FeCO}_3$ , resulting in the formation of grape-like siderite and infiltrated sand aggregates. Siderite formed during this stage exhibits the highest purity, with the highest content in its chemical composition being of  $\text{Fe}_2\text{O}_3^{\text{T}}$ , while  $\text{SiO}_2$ ,  $\text{Al}_2\text{O}_3$ ,  $\text{TiO}_2$ , and other elements are relatively low. This may be attributed to the prior presence of saline-rich connate water or weakly acidic groundwater in sedimentary pore spaces, capable of dissolving metal minerals and allowing dispersed iron to precipitate as  $\text{FeCO}_3$  after short-distance water dissolution and transport. As a result, the mineral composition undergoes purification and enrichment. These phenomena result from siderite dissolution during the diagenetic phase and subsequent reprecipitation in regional tensile fractures during the diagenetic period of sedimentary strata.

## 6. Conclusions

Fieldwork and laboratory investigations supported the classification of siderite, in the Late Permian Xuanwei Formation coal-bearing strata of the eastern Yunnan region, into four distinct types. Stratiform-laminated siderite: This type displays shades from bluish-gray to dark gray and is composed of uniform, fine-crystalline siderite, and peat—it exhibits distinctive laminae and layered structures. Lens-nodular siderite: This variant appears gray-yellow and comprises micritic siderite, medium to coarse crystalline semi-autochthonous siderite, and oolitic chlorite—it shows a conformable distribution. Siderite as sandstone cement: In this category, the siderite is yellow-brown and consists of dispersed siderite aggregates and massive siderite clasts—it fills intergranular pores between debris particles in the form of cement. Siderite filling in fractures: This type generally occurs in grape-like or mesh-like structures, intersecting the strata at large angles—it exhibits a crystal grain structure of varying grain sizes and has the highest purity among the four types.

Under reducing conditions, stratiform-laminated and lens-nodular siderite form through sedimentation in iron-rich marine–terrestrial transitional environments. Siderite cement in sandstone forms through cementation and precipitation within the intergranular pores of debris particles under reducing conditions. Siderite developed in structural fractures is formed within vertical fractures that began during the Yanshan orogeny. This

results from the dissolution of siderite during the diagenetic phase in the sedimentary strata and its subsequent reprecipitation in regional tensile fractures.

**Author Contributions:** Conceptualization, H.T. and B.L.; methodology, H.T. and B.L.; formal analysis, H.T. and B.L.; investigation, H.T., Q.Z., B.L. and K.S.; writing—original draft preparation, H.T.; writing—review and editing, H.T. and S.T.; visualization, H.T. and Q.Z.; supervision, B.L.; project administration, K.S. All authors have read and agreed to the published version of the manuscript.

**Funding:** This research was funded by SINOPEC Exploration Company, grant number 35450003-21-ZC0607-0003, Yunnan Fundamental Research Projects (grant number: 202301BF070001-020), Yunnan Key research and development plan program (grant number: 202303AP140020) and Yunnan University Graduate Research Innovation Project (grant number: KC-22223123).

**Conflicts of Interest:** The authors declare no conflict of interest.

## References

- Huang, L.P. On Siderite in Tongziyan Formation, Longyong Coalfield and Its Lithofacies Meaning. *Coal Geol. China* **2004**, *51*, 41–43. (In Chinese)
- Ohmoto, H.; Watanabe, Y.; Kumazawa, K. Evidence from massive siderite beds for a CO<sub>2</sub>-rich atmosphere before approximately 1.8 billion years ago. *Nature* **2004**, *429*, 395–399. [[CrossRef](#)] [[PubMed](#)]
- Sengupta, R.; Tosca, N.J.; Robinson, S.A. Geochemical controls on the elemental composition of siderite: Implications for palaeo-environmental reconstructions. *Geochim. Cosmochim. Acta* **2019**, *271*, 1–15. [[CrossRef](#)]
- Jiang, C.Z.; Halevy, I.; Tosca, N.J. Kinetic isotope effect in siderite growth: Implications for the origin of banded iron formation siderite. *Geochim. Cosmochim. Acta* **2022**, *322*, 260–273. [[CrossRef](#)]
- Liu, B.J.; Xu, X.H.; Yu, G.M. A preliminary study of the depositional environment and formation of layer-controlled clinopyroxene deposits. *J. Chengdu Coll. Geol.* **1980**, *2*, 3–10. (In Chinese)
- Li, T. Metallogenic geochemistry of marine sedimentary siderite deposits. *Geol. Explor.* **1979**, *1*, 1–8. (In Chinese)
- Xie, B.Z.; Sun, L.F.; Fang, H.; Shi, X.Y.; Tang, D.J. Siderite in banded iron formation of the Neoproterozoic Baizhiyan Formation, Shanxi Province: Genesis and palaeoenvironmental implications. *J. Palaeogeogr.* **2021**, *23*, 175–190. (In Chinese)
- Zhang, Z.C.; Hou, T.; Chen, Z.G. Mineralization related to large igneous provinces. *Acta Geol. Sin.* **2022**, *96*, 131–154. (In Chinese)
- Zhang, T.; Shen, Y.L.; Li, Z.F.; Jin, J.; Zong, Y.; Liu, J.B.; Zheng, J. Genesis of Siderite Precipitated in the Lopingian Coal Measures in Zhijin Mining Area, Western Guizhou. *Geol. J. China Univ.* **2018**, *24*, 481–490. (In Chinese) [[CrossRef](#)]
- Dong, Z.H.; Huang, H.Q. Cementation characteristics of siderite in sandstone and siltstone. *Mineral. Petrol.* **1980**, *2*, 60–62+113–115. (In Chinese) [[CrossRef](#)]
- Raiswell, R.; Reinhard, C.T.; Derkowski, A.; Owens, J.; Bottrell, S.H.; Anbar, A.D.; Lyons, T.W. Formation of syngenetic and early diagenetic iron minerals in the late Archean Mt. McRae Shale, Hamersley Basin, Australia: New insights on the patterns, controls and paleoenvironmental implications of authigenic mineral formation. *Geochim. Cosmochim. Acta* **2011**, *75*, 1072–1087. [[CrossRef](#)]
- Liao, S.F.; Liang, T.R.; Zeng, M.G. Geochemical characteristics of gossan related to Siderite deposits in carbonate strata, western Guizhou. *Geochimica.* **1980**, *4*, 323–332. [[CrossRef](#)]
- Shao, L.Y.; Zhang, P.F.; Chen, D.Z.; Luo, Z. Braided Delta Depositional System and Coal Accumulation During Early Late Permian Period in Eastern Yunnan and Western Guizhou, Southwest China. *Acta Sedimentol. Sin.* **1994**, *4*, 132–139. (In Chinese)
- Long, J.F. Study of Siderite in Sedimentary Strata of the Coal-containing. *J. Huainan Min. Inst.* **1986**, *1*, 97–102+105. (In Chinese)
- Shen, Y.L.; Qin, Y.; Li, Z.F.; Jin, J.; Wei, Z.H.; Zheng, J.; Zhang, T.; Zong, Y.; Wang, X.H. The sedimentary origin and geological significance of siderite in the Longtan Formation of western Guizhou Province. *Earth Sci. Front.* **2017**, *24*, 152–161. (In Chinese) [[CrossRef](#)]
- Shen, Y.L.; Qin, Y.; Guo, Y.H.; Yi, T.S.; Yuan, X.X.; Shao, Y.B. Characteristics and sedimentary control of a coalbed methane-bearing system in Lopingian (late Permian) coal-bearing strata of western Guizhou Province. *J. Nat. Gas Sci. Eng.* **2016**, *33*. [[CrossRef](#)]
- Zhao, Q.; Dai, X.Y.; Liu, B.; Tang, H.L.; Quan, G.L. Characteristics of tight gas reservoir in sequence framework of Permian Longtan Formation in eastern Yunnan-western Guizhou area, China. *J. Chengdu Univ. Technol. (Sci. Technol. Ed.)* **2022**, *49*, 12–23. (In Chinese) [[CrossRef](#)]
- Shen, Y.; Qin, Y.; Wang, G.G.X.; Xiao, Q.; Shen, J.; Jin, J.; Zhang, T.; Zong, Y.; Liu, J.; Zhang, Y. Sealing capacity of siderite-bearing strata: The effect of pore dimension on abundance and micromorphology type of siderite in the Lopingian (late Permian) coal-bearing strata, western Guizhou province. *J. Pet. Sci. Eng.* **2019**, *178*, 180–192. [[CrossRef](#)]
- Liu, D.M.; Jia, Q.F.; Cai, Y.D. Research progress on coalbed methane reservoir geology and characterization technology in China. *Coal Sci. Technol.* **2022**, *50*, 196–203. (In Chinese)
- Ming, L.S.; Dai, S.F.; David, I.T.; Graham, B.F.; Wang, N.; Tian, X. Geochemical and mineralogical evidence for the formation of siderite in Late Permian coal-bearing strata from western Guizhou, SW China. *Chem. Geol.* **2023**, *637*, 121675.
- Li, J.H.; Ma, Z.L.; Zhang, Y.Q.; Dong, S.W.; Li, Y.; Lu, M.A.; Tan, J.Q. Tectonic evolution of Cretaceous extensional basins in Zhejiang Province, eastern South China: Structural and geochronological constraints. *Int. Geol. Rev.* **2014**, *56*, 1602–1629. [[CrossRef](#)]

22. Dou, X.Z. Tectonic Evolution and Its Control on Coalbed Methane Reservoiring in Western Guizhou. Doctor's Thesis, China University of Mining and Technology, Xuzhou, China, 2012. (In Chinese).
23. Wang, J. The Geochemistry of the coals at P/T boundary in Xuanwei, Yunnan and its Paleoenvironmental significance. Doctor's Thesis, China University of Mining and Technology, Beijing, China, 2015. (In Chinese).
24. He, B.; Xu, Y.G.; Chung, S.L.; Xiao, L.; Wang, Y. Sedimentary evidence for a rapid, kilometer-scale crustal doming prior to the eruption of the Emeishan flood basalts. *Earth Planet. Sci. Lett.* **2003**, *213*, 391–405. [[CrossRef](#)]
25. Wang, X.; Shao, L.; Eriksson, K.A.; Yan, Z.; Wang, J.; Li, H.; Zhou, R.; Lu, J. Evolution of a plume-influenced source-to-sink system: An example from the coupled central Emeishan large igneous province and adjacent western Yangtze cratonic basin in the Late Permian, SW China. *Earth-Sci. Rev.* **2020**, *207*, 103224. [[CrossRef](#)]
26. Xie, J.R. Introduction to Yunnan Mineral Resources. *Geol. Rev.* **1941**, *6*, 1–42+219. (In Chinese) [[CrossRef](#)]
27. Yunnan Geological and Mineral Bureau. *Regional Geological Records of Yunnan Province*; Geological Publishing House: Beijing, China, 1990. (In Chinese)
28. Dai, H.W.; Chen, M.S.; Chen, W.M. The Study of Coal-bearing substances of Different ages and coal features in China. *J. Fuel Chem. Technol.* **1981**, *1*, 1–13. (In Chinese)
29. Qian, D.D.; Wei, B.X.; Li, Y. *General Introduction of Coal Resources in China*; Geological Publishing House: Beijing, China, 1996. (In Chinese)
30. Rasmussen, B.; Muhling, J.R. Syn-tectonic hematite growth in Paleoproterozoic Stirling Range “red beds”, Albany-Fraser Orogen, Australia: Evidence for oxidation during late-stage orogenic uplift. *Precambrian Res.* **2019**, *321*, 54–63. [[CrossRef](#)]
31. Qiu, Z.G. Division of genetic subtypes of sedimentary deposits and genesis of sedimentary siderite. *Miner. Depos.* **1987**, *1*, 68–78. (In Chinese)
32. Dai, S.; Bechtel, A.; Eble, C.F.; Flores, R.M.; French, D.; Graham, I.T.; Hood, M.M.; Hower, J.C.; Korasidis, V.A.; Moore, T.A.; et al. Recognition of peat depositional environments in coal: A review. *Coal Geol.* **2020**, *219*, 103383. [[CrossRef](#)]
33. Sugitani, K.; Horiuchi, Y.; Adachi, M.; Sugisaki, R. Anomalously low Al<sub>2</sub>O<sub>3</sub>/TiO<sub>2</sub> values for Archean cherts from the Pilbara Block, Western Australia—Possible evidence for extensive chemical weathering on the early earth. *Precambrian Res.* **1996**, *80*, 49–76. [[CrossRef](#)]
34. Xu, Y.; Chung, S.L.; Jahn, B.M.; Wu, G. Petrologic and geochemical constraints on the petrogenesis of Permian–Triassic Emeishan flood basalts in southwestern China. *Lithos* **2001**, *58*, 145–168. [[CrossRef](#)]
35. Lai, S.; Qin, J.; Li, Y.; Li, S.; Santosh, M. Permian high Ti/Y basalts from the eastern part of the Emeishan Large Igneous Province, southwestern China: Petrogenesis and tectonic implications. *J. Asian Earth Sci.* **2012**, *47*, 216–230. [[CrossRef](#)]
36. Xu, Y.G.; Chung, S.L.; Shao, H.; He, B. Silicic magmas from the Emeishan large igneous province, Southwest China: Petrogenesis and their link with the end-Guadalupian biological crisis. *Lithos* **2010**, *119*, 47–60. [[CrossRef](#)]
37. Wedepohl, K.H. The Composition of the Continental Crust. *Geochim. Cosmochim. Acta* **1995**, *59*, 1217–1232. [[CrossRef](#)]
38. Yang, J.; Cawood, P.A.; Du, Y. Voluminous silicic eruptions during late Permian Emeishan igneous province and link to climate cooling. *Earth Planet. Sci. Lett.* **2015**, *432*, 166–175. [[CrossRef](#)]
39. Ali, J.R.; Thompson, G.M.; Zhou, M.; Song, X. Emeishan large igneous province, SW China. *Lithos* **2005**, *79*, 475–489. [[CrossRef](#)]
40. Zhang, C.Q. The Genetic Model of Mississippi Valley-Type Deposits in the Boundary Area of Sichuan, Yunnan and Guizhou Provinces, China. Doctor's Thesis, Chinese Academy of Geological Sciences, Beijing, China, 2008. (In Chinese)

**Disclaimer/Publisher's Note:** The statements, opinions and data contained in all publications are solely those of the individual author(s) and contributor(s) and not of MDPI and/or the editor(s). MDPI and/or the editor(s) disclaim responsibility for any injury to people or property resulting from any ideas, methods, instructions or products referred to in the content.